Chapter 6

Simulation of gas-solid flow in airlift conveyor

6.1 Problem and objective

In this chapter, gas-solid particle flow of industrial scale airlift conveyor in powder detergent plant is simulated using the mathematical model and computational method discussed in previous chapter. An airlift conveyor can be categorized as vertical pneumatic conveyor and is utilized to convey detergent powder from spray dryer to further screening process as the diagram shown in figure1.1. The detergent powders contain 7 to 10% moisture flow upward in the pipe due to negative suction pressure created by a centrifugal blower. Some of powders collide with the wall and then adhere to the wall due to its moisture and stickiness. The higher concentration of powders near pipe wall induce the higher possibility of sticking. Pipe clogging thus occurs after a period of deposition.

This engineering problem has been solved by various methods. Slit wall method utilize many smooth plastic strip arranged in circular pipe configuration, each strip overlap to the other, allowing air to pass between overlapping space between each strip to purge the powder away from wall. The other method utilize a flexible wall such as cloth wall with a cam-operating vibrator mounted on the wall.

In this chapter, a cost effective modification of airlift inlet configuration is proposed in order to reduce rate of powder deposition on pipe wall. The CFD technique and the mathematical model discussed in previous chapter will be applied to study effects of pipe inlet configurations to powder concentration and mass rate of particle-wall collision in acceleration zone of vertical airlift pipe in order to evaluate the most appropriate inlet configuration.

6.2 Airlift conveyor geometry and operating conditions

It is hereby agree that exact plant' information is confidential, a scale down airlift conveyor is therefore presented here. However, the characteristic flow parameters of the scale down airlift still contain physical realistic information as of actual airlift.

Pipe geometry

Pipe diameter	0.2 m
Pipe length	7.0 m

Table 6.1

Material property of carrier phase

Air density	1.178 Kg/m^3
Air laminar viscosity	1.868*10^{-5}Kg/m.s

Table 6.2

Material property of dispersed phase

Density of spray dried detergent powders can not be measured in straight forward manner. According to evaporation during spray drying, a powder contain many micropores created by bursting of vaporized water. When cooling down, the micropores are then replaced with air. The volume of these micropores cause difficulty in measuring "true" density of a sprayed dried powders. However, if the volume of water evaporated is assumed to be replaced by equal volume of air, powder density can be approximated based on this assumption resulting in ρ_p=825 kg/m^3.

Powder is assumed uniform in size, although particle size distribution in actual plant operation is wide, the nominal size is chosen so that d_p= 500 μm . In summary;

Particle density, ρ_p	825 kg/m^3
Particle size, d_p	500 μm

Table 6.3

Air inlet velocity

Air inlet velocity is specified by the optimal velocity operated in actual unit. There are two criteria in operating the actual airlift unit, first, the inlet air velocity should be high enough to pick up most of "nominal" size powder, second, inlet air velocity should not be so high until too large or agglomerated powder is picked up into the pipe. The optimum inlet velocity of 14-16 m/s for solid loading ratio 1.0-1.2 is reported, subjected to actual plant operating condition. In this study Air velocity is specified to 16 m/s.
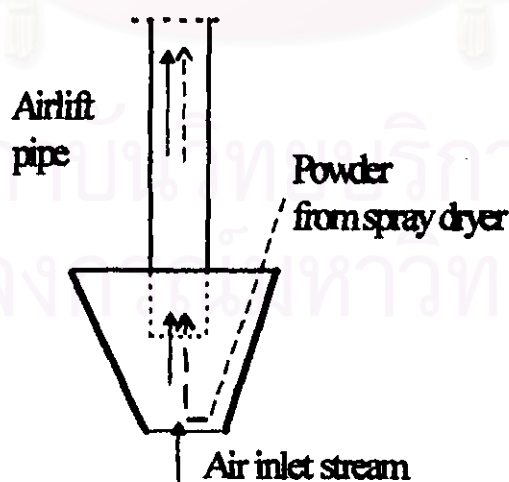
Particle inlet velocity

Figure 6.1
Feeding section of airlift conveyor

Figure 6.1 illustrates feeding section of airlift system. Air is assumed to enter in to the system via opening at the bottom of the hopper where it coincides with the powders poured down from the top opening of the hopper. Interphase momentum transfer from air to powders reverses the direction of the powders and accelerate it toward the pipe inlet. If the distance between bottom opening of hopper and pipe inlet is known, inlet particle velocity can be calculated using Morsi and Alexander [1972] 's calculation method given in equation (3.50) through (3.55). In this study, the distance between bottom opening and pipe inlet is specified to 25 cm. Setting the initial particle velocity at the bottom opening of hopper equal to zero and insert material properties specified in Table 6.3 together with air inlet velocity V_g=16.00 m/s into equation (3.50) through (3.55) and then solve for particle velocity. Following trial and error calculation, results in inlet particle velocity V_p=10.5 m/s. The solid loading ratio is specified to 1.2. In summary;

Operating condition

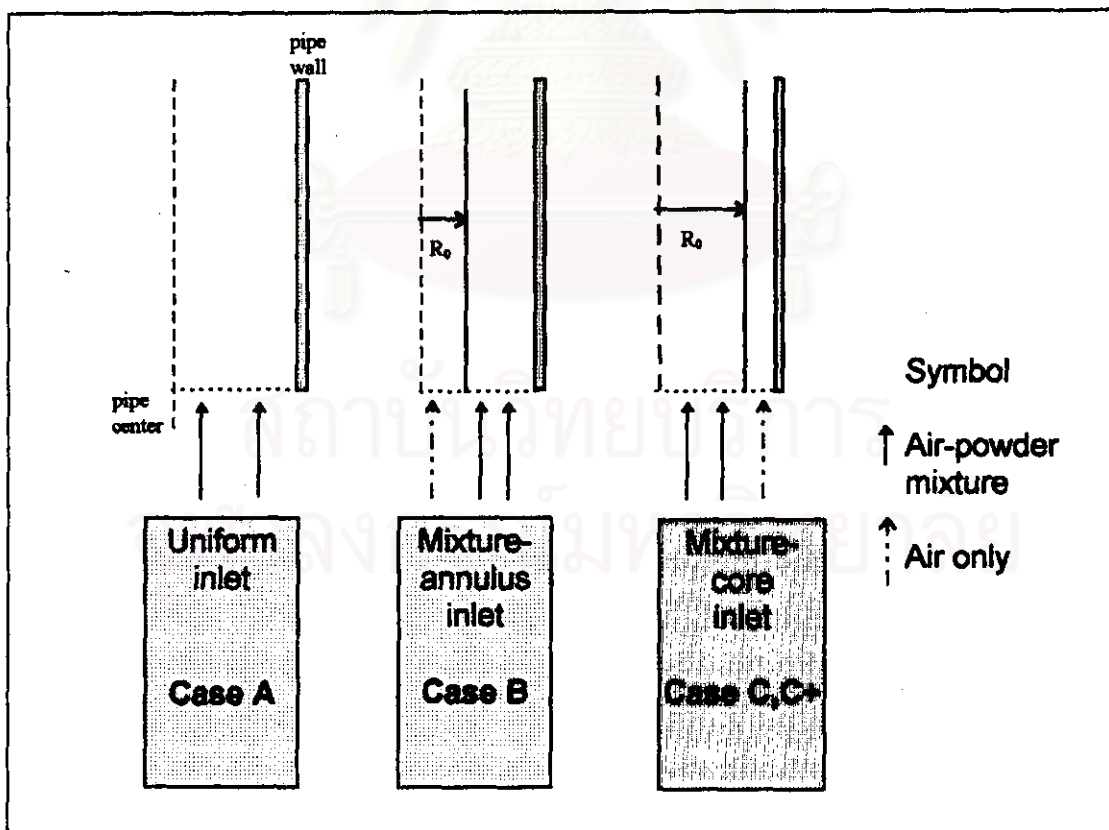| Inlet air velocity	16.0 m/s
Inlet particle velocity	10.5 m/s
Solid loading ratio	1.2

Table 6.4

6.3 Proposed inlet configurations

Figure 6.2
Proposed inlet configurations

Three proposed inlet configurations are illustrated in Figure 6.2. The walls of pipe are shown by solid lines. The pipe inlets are shown as broken line. The word "mixture" represents air-powder mixture.

For uniform inlet configuration (Case A), it is assumed that volume fraction of particle and air are uniform throughout the cross section of pipe inlet. This is the reference case which represent for actual unit.

For mixture-annulus inlet configuration (Case B) in Figure 6.2, mixture of air-powder enters in annular region ($R_0 < r < R_t$) and a stream of air only enter in core region. Inlet particle volume fraction and velocity are assumed uniform for entire annular inlet region. Inlet air velocity is assumed uniform and equal for entire core and annular inlet region.

For mixture-core inlet configuration (Case C and C+) in Figure 6.2, mixture of air-powder enters in pipe core region ($0 < r < R_0$) and a stream of air only enter in annular region. Inlet particle volume fraction and velocity are assumed uniform for entire core region. Inlet air velocity is assumed uniform and equal for entire core and annulus region.

Mixture-annulus inlet (Case B) and mixture-core inlet (Case C) flow are proposed to evaluate the resulting powder concentration (volume fraction) near by wall. For mixture-annulus inlet, powders are expected to diffuse from annulus to core region due to volume fraction gradient. If particle diffusion rate is high enough, particle concentration at pipe wall should be gradually reduced in comparison with uniform inlet case. For mixture-core inlet (Case C), lower particle volume fraction in annular region at the inlet cause particles to be accelerated in axial direction at higher rate within such region than those of uniform inlet case. At the same time, there are particles diffuse from the core region to annular region in radial direction due to volume fraction gradient. If particle axial convection flux (mass rate per unit area due to convection) is higher than particle radial diffusion flux, number of particles reach to the wall are expected be reduced in comparison with uniform inlet case.

6.4 Computational details

In order to study particle concentration and its collision rate to the pipe wall, the computational cell adjacent to the wall boundary should be in proper size. For computational purpose, the wall function method can be applied when each computational node adjacent to the wall is located within $30 \leq y^+ \leq 130$. For y^+ calculation, total pressure per pipe length of a uniform inlet airlift is computed first by CFD technique using coarse radial grid, since total pressure is insensitive to radial grid arrangement. Wall shear stress τ_0 can then be calculated by subtracting computed total pressure drop per pipe length by gravity force per unit volume and multiply the result with 0.5*R. Substitute other air property in Table 6.2 and the resulting τ_0=2.42 N/m^3 to equation (3.24) and (3.25) together with the desired value of y^+ which is specified to 45, as a result, computational grid node distance adjacent to pipe wall is (R-r)=0.5mm.

Axial grid distance is uniform and can be specified on the same basis as computation cases in chapter 5. Pipe geometry, material properties and boundary conditions are specified as in Table 6.1 through 6.4. The validated model in chapter 5 including turbulence phase mass diffusion term is employed in computation. The model is solved using IPSA with elliptic-parabolic mixed solution procedure. With reference of Figure 6.2, computational detail for each case are summarized in table 6.5.

Inlet configuration	A	B	C	C+
Total non-uniform radial grids, NY	40	40	40	40
$NY(R_0)$	40	5	30	23
R_0	.10	.04353	.08913	.08014
Mixture flow area (A_m)	.031416	.02546	.0250	.0202
local solid loading ratio	1.2	1.4807	1.507	1.8663
Total solid loading ratio	1.2	1.2	1.2	1.2

Table 6.5

For all cases, amount of axial grids are 70 for total length 7.00 m. The radial distance between last radial grid node and pipe wall is 0.5 mm in all cases. Radial grid arrangement is illustrated in Figure 6.3

2-PHASE AIR-SOLIDS UNIFORM INLET AIRLIFT
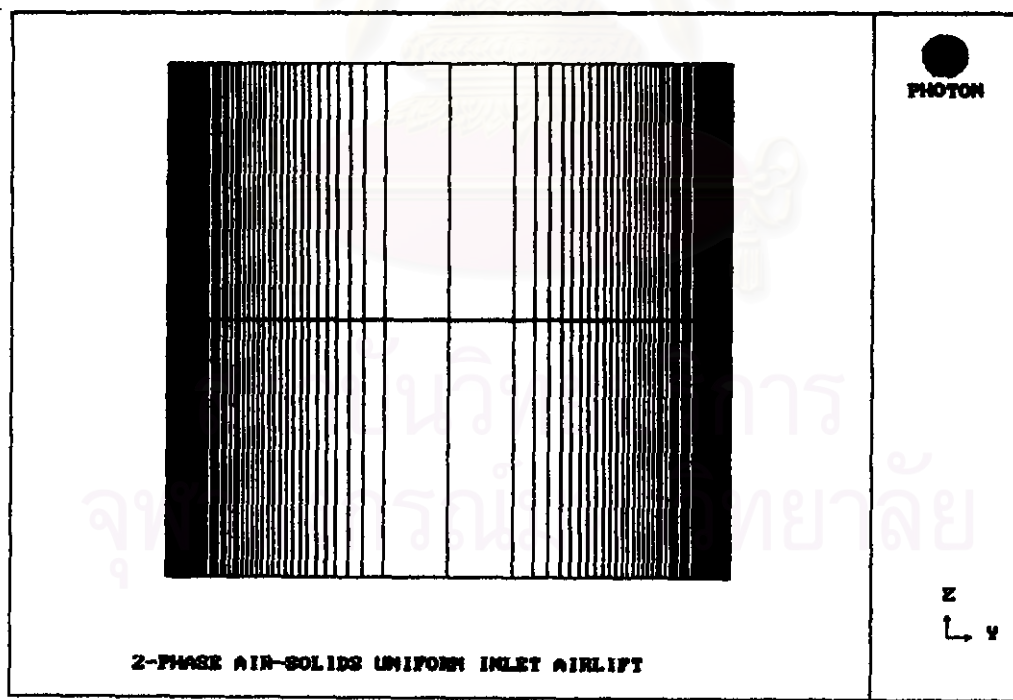
Figure 6.3
Non uniform computational radial grid used in airlift inlet configuration study
total grid in radial direction NY=40 (half of diameter), total uniform grid in axial direction NZ=70

Q1 Instruction files for Case A, B, C and C+ are attached here in Appendix B4 through B7.

6.5 Discussion of computational result

6.5.1 Mechanism of powder deposition on vertical wall

In the model validation studied in previous chapter, particle-wall interaction force was negligible as it did not significantly affect the particle flowfield. In fact, in a negligible electrostatic field force flow of non-sticky particle in vertical pipe, the particle deposition on pipe wall is rarefied. However, in this study, the flow of sticky powders in vertical pipe come into question. Powder deposition on the wall indeed occur due to powder collisions on the pipe wall. Evaluation of deposition rate of the proposed configuration flows require mathematical index to indicate the strength of collision rate and strength of lift force per unit mass in which reentrainment of powder back to main air stream may occur.

Soo[1967] defined mass rate of particle collision to wall per unit area as follows;

$$M_{pw} = \frac{1}{4}\gamma_p \rho_p \sqrt{v_p'^2} \tag{6.1}$$

This mass rate of particle collision can be determined experimentally by mounting a set of double side scotch tape which its area is known in vertical pipe wall and then counting the amount of particles adhere on the tape after certain period of time. The above equation (6.1) is also suggested by investigator such as Laufer [1954] on such experiment. Although particle r.m.s fluctuating velocity v_p' could not be independently predicted, it can be compared with particle phase mass diffusivity term in the equation (3.32) if the corresponding computational grid node is located close enough to the wall. Finally;

$$\text{collision rate index} = C\left(\gamma_p \rho_p k^2 / \varepsilon\right)\Big|_{\text{boundary cell}} \tag{6.2}$$

Where C is constant and the other terms are corresponding to terms in equation (3.32).

Lift force per unit mass of particle play an important role in determining rate of deposition of sticky powder . Higher lift force per unit mass of particle, higher possibility of slipping or rebounding of particles on wall or deposited layer. Mathematical expression of Lift force per unit mass is given in Soo [1982] using correlation factor of Saffman [1965] as follows;

$$f_L = -\frac{3}{8}\left(\frac{12.92}{\pi}\sqrt{\mu \frac{dv_x}{dy}}\right)\frac{\rho}{\rho_p}\frac{|v_w|}{d_p} \tag{6.3}$$

Where

$$V_w = \left[v_p - v_a + \left(2d_p \frac{dv_a}{dy}\right)\right] \tag{6.4}$$

The term $\sqrt{\mu \dfrac{dv_s}{dy}|V_{sl}|}$ of boundary cell will be used as lift force index for evaluation.

6.5.2 Discussion of computational result: effect of inlet configuration

6.5.2a. Velocity profile

In Figure 6.4 through 6.9, computed air and powder velocity profile of three inlet configuration flows are plotted at various pipe lengths of acceleration region. The velocity distribution of both phases are plotted in order from the position of 1.00 m pipe length in Figure 6.4 to 6.00 m pipe length in Figure 6.9. Computed air velocity of uniform inlet (Case A) exhibit a straight line profile in almost entire section of pipe except near-wall region. Curved profile is developed and centerline air velocity increases along the axial direction. The same characteristic can be found in particle velocity profile.

Computed air velocity profile of mixture-annulus inlet configuration flow (Case B) is quite different from the uniform inlet case. The clean air flow in core region cause maximum centerline velocity at the starting section and decrease along axial direction. Particle shear stress transfer from center line toward the pipe wall at the highest rate among the three case as can be observed by the steepest particle velocity gradient.

Computed air velocity profile of mixture-core inlet configuration (Case C) exhibit concave curve in the core region. There is an area of relative high particle velocity which tend to move toward the pipe centerline as the flow move upward along axial direction. Particle velocities near by pipe wall of this case are the highest among the three cases in the entire length considered, which may indicate more "dilute" flow near wall than the other cases.

Air velocity gradients in near-wall region of acceleration zone of the three cases are approximately equal, for example, in Figure 6.4, difference of air velocity gradients in near-wall region do not exceed 5%. Air velocity gradient term in equation (6.3) and (6.4) is therefore considered constant for the three cases. The remaining term used as lift force index is slip velocity. Particle Reynolds number (equation (3.36)) can then be considered as representative for lift force index.
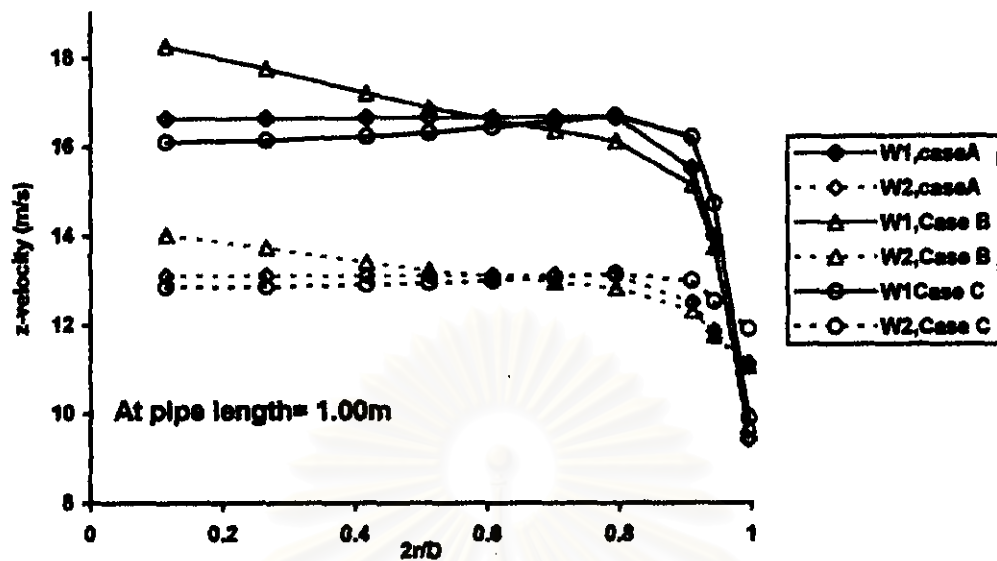
Figure 6.4

Computed result of air velocity profile (W1) and particle velocity profile (W2) on radial variation at z=1.00m . Data legend: Case A denote uniform inlet configuration flow ; Case B denote mixture-annulus inlet configuration flow; Case C denote mixture-core inlet configuration flow. The simulation parameters are listed in Table 6.1 through 6.5
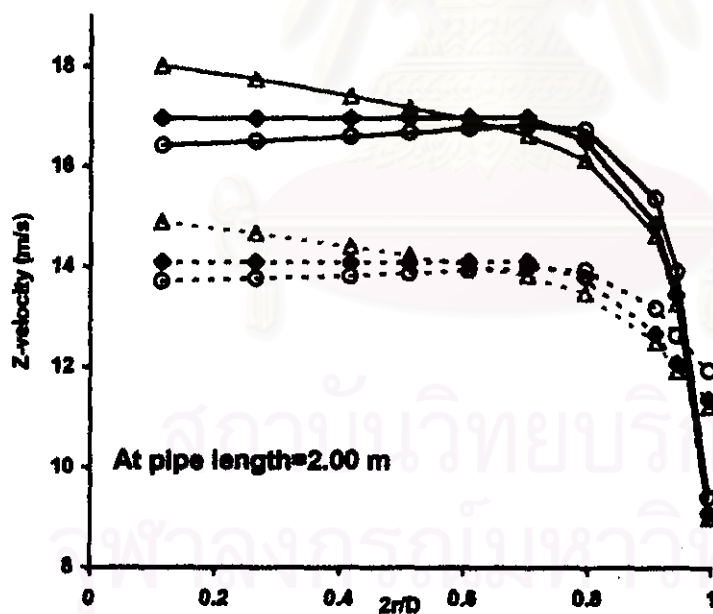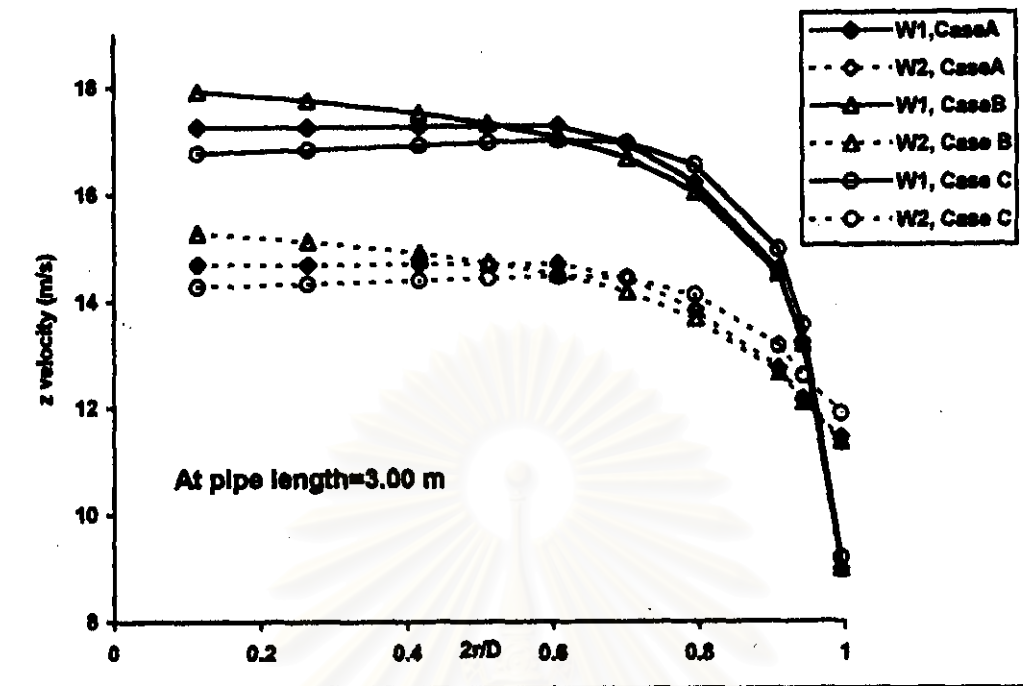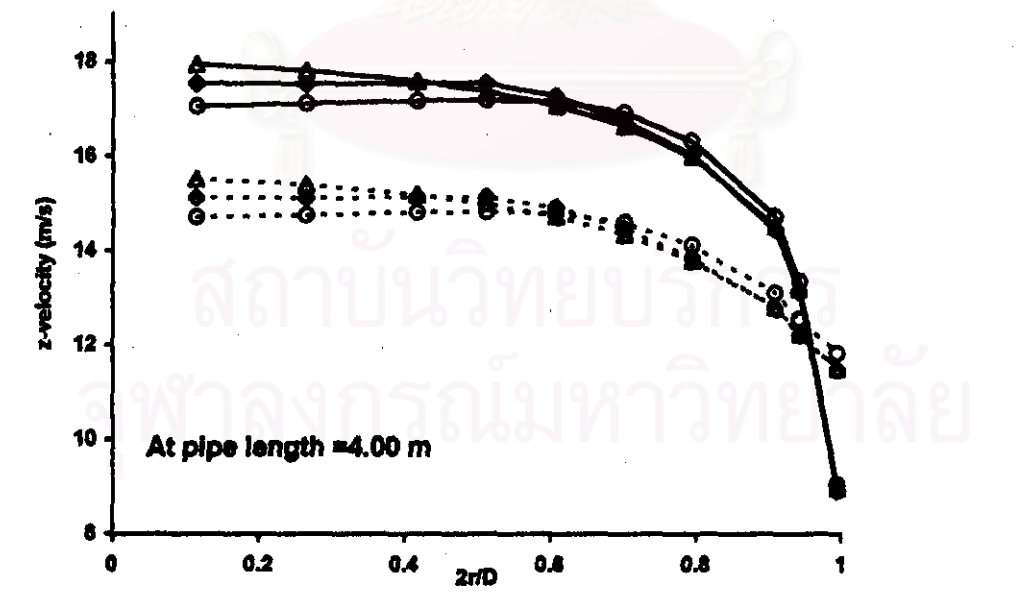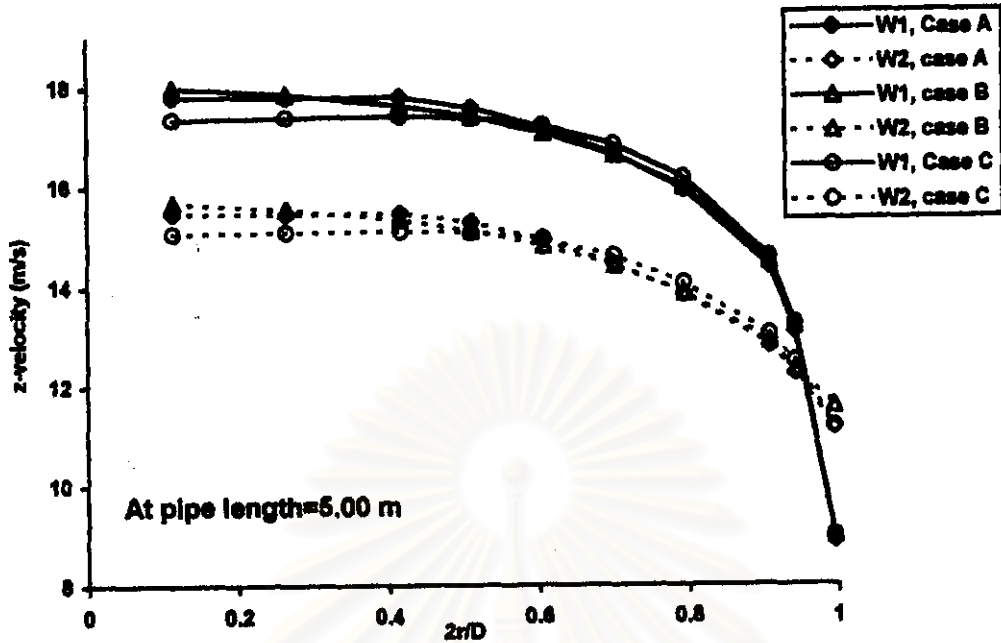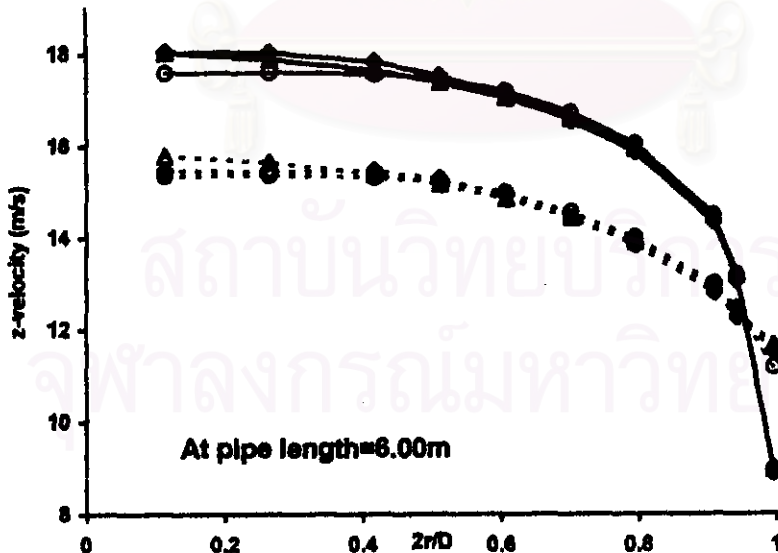

Figure 6.5

Computed result of air velocity profile (W1) and particle velocity profile (W2) on radial variation at z=2.00m . Data legend: similar to Figure 6.4.

Figure 6.6
Computed result of air velocity profile (W1) and particle velocity profile (W2) on radial variation at z=3.00m . Data legend: Case A denote uniform inlet configuration flow ; Case B denote mixture-annulus inlet configuration flow; Case C denote mixture-core inlet configuration flow. The simulation parameters are listed in Table 6.1 through 6.5

Figure 6.7
Computed result of air velocity profile (W1) and particle velocity profile (W2) on radial variation at z=4.00m . Data legend: similar to Figure 6.6.

Figure 6.8

Computed result of air velocity profile (W1) and particle velocity profile (W2) on radial variation at z=5.00m . Data legend: Case A denote uniform inlet configuration flow ; Case B denote mixture-annulus inlet configuration flow; Case C denote mixture-core inlet configuration flow. The simulation parameters are listed in Table 6.1 through 6.5

Figure 6.9

Computed result of air velocity profile (W1) and particle velocity profile (W2) on radial variation at z=6.00m . Data legend: similar to Figure 6.8.

6.5.2b. Volume fraction

Figure 6.10through 6.13 illustrate contour plot of computed particle volume fraction distribution in acceleration zone of uniform inlet configuration case. Particle volume fraction contour are plotted in each pipe section of 1.00 to 1.10 m length in each Figure due to limitation of the PHOTON graphic module. The pipe sections are presented in order from 0.00-1.00 in Figure 6.10 to 2.90-4.00 m in Figure 6.13. The particle volume fractions are almost radial uniform but axially decrease in order to conserve its mass flux since velocity increase along the axial direction. Particle volume fraction reaches a constant at z = 4.00 m, approximately.

As the flow move upward along axial direction, particle volume fraction at the wall region start to be lower than volume fraction in turbulence core region as can be observed from Figure 6.11. This phenomena arise due to effect of particle shear stress term which, due to higher particle velocities in core region, the particle momentum transfer from core region toward pipe wall, as a result, near-wall particles are accelerated in the higher rate than that of the core region. The near-wall particle volume fractions therefore decrease in the higher rate than that of inner region.

From Figure 6.10, there appear an area of relative high concentration in a pipe cross section which locate near by the pipe wall. The relative high concentration area tend to be smaller and its location is simultaneously get nearer toward pipe centerline as the flow moves upward along axial direction as can be seen in order from Figure 6.10 through 6.13. The area of relative high concentration is created by effect of particle phase mass diffusion. At the inlet, particle velocities near wall are lower than those in the core section according to lower air velocities, the particle volume fraction of the near-wall cells are therefore maximum. The particle volume fraction gradient between near-wall region and the inner area cause particles to diffuse from the wall toward pipe center at the starting section of acceleration zone where volume fraction gradients between core region and near-wall region are large.

Figure 6.14 through 6.17 illustrate particle volume fraction distribution contour of mixture-annulus inlet configuration case (Case B). The contour plot in 1.00 to 1.10 m pipe section per Figure are presented in order from pipe inlet to 4 m length in Figure 6.14 through 6.17. Particles diffuse from annular region to core region due to volume fraction gradient until it reach radial uniform at z=4 m. Particle volume fractions near wall decrease as the flow moves upward due to diffusion of particles to core region and acceleration of particles along axial direction.

Figure 6.18 through 6.21 illustrate particle volume fraction distribution contour of mixture-core inlet configuration case (Case C). The contour plot in 1.00 to 1.10 m pipe section per Figure are presented in order from pipe inlet to 4 m length in Figure 6.18 through 6.21. As the flow move upward, particles diffuse from core region toward the wall, cause near-wall particle volume fractions to increase, simultaneously, acceleration of near-wall particles along axial direction cause near-wall particle volume fractions to decrease. The net effect will be investigated later.
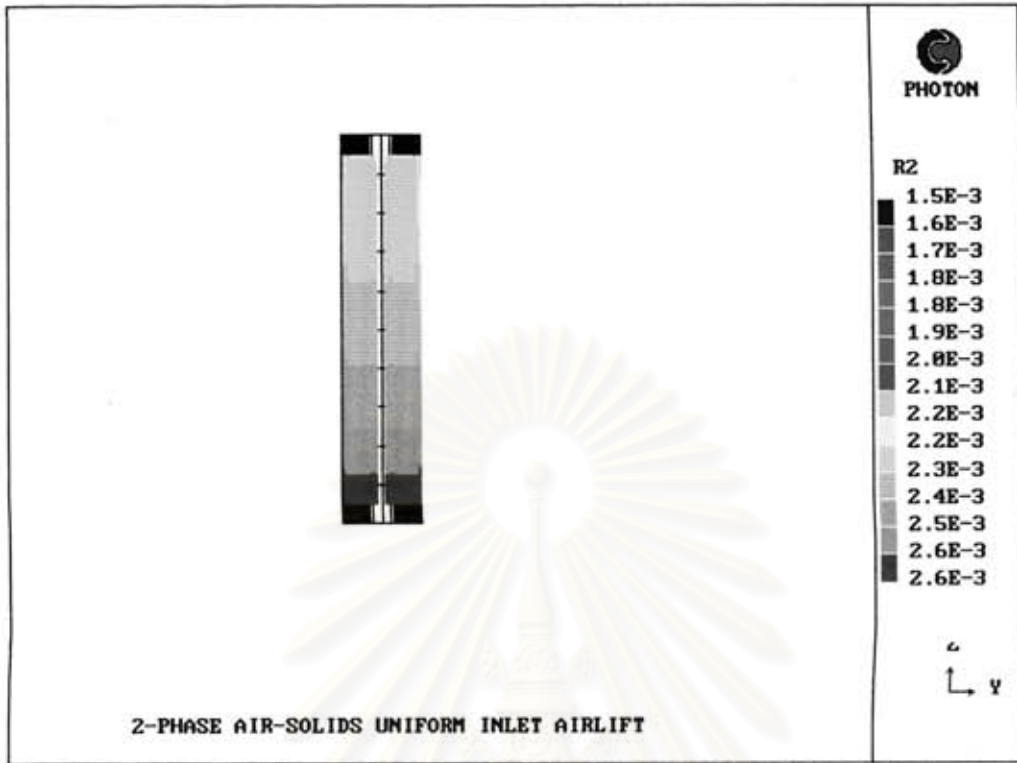
Figure 6.10
Solid volume fraction contour line for case A (uniform inlet)
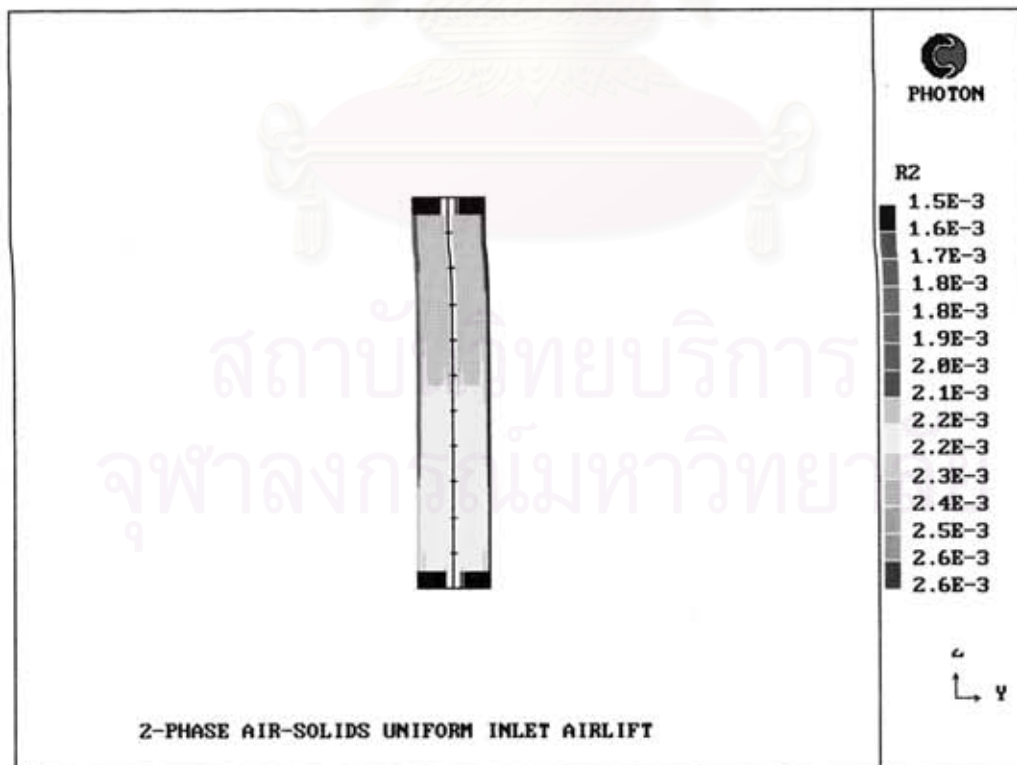from NZ=1 to NZ=10 (Zmin =0.0m ,Zmax=1.00 m)

Figure 6.11
Solid volume fraction contour line for case A (uniform inlet)
from NZ = 10 to NZ=20 (Zmin =0.9m ,Zmax=2.00 m)

Figure 6.12
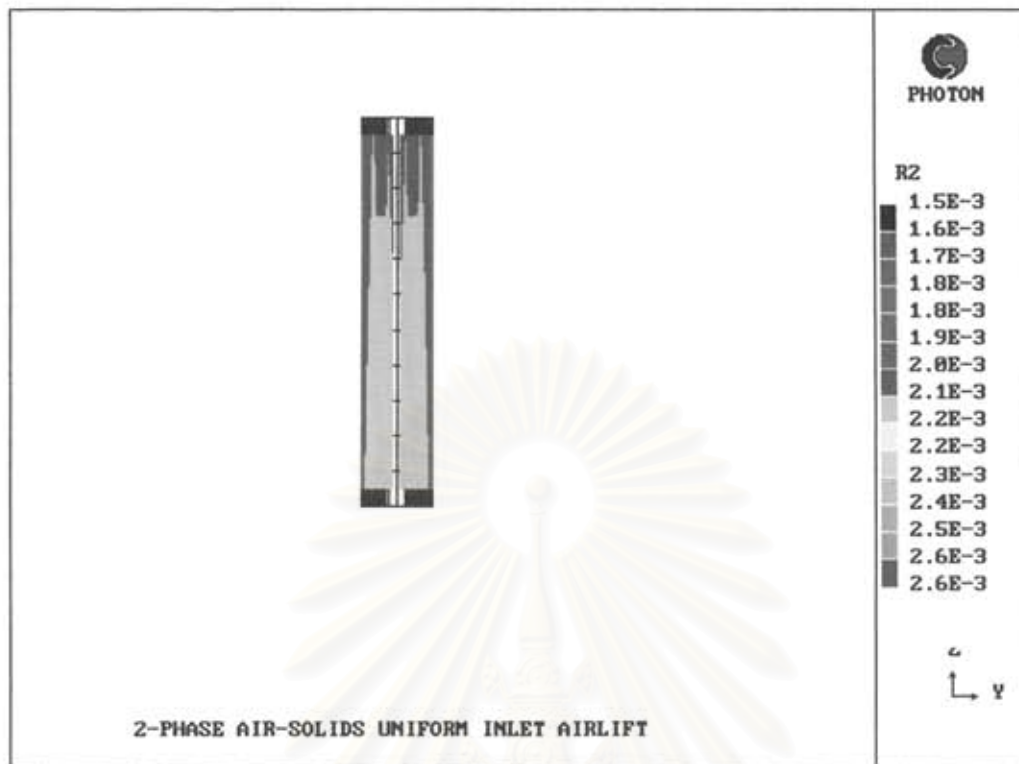Solid volume fraction contour line for case A (uniform inlet)
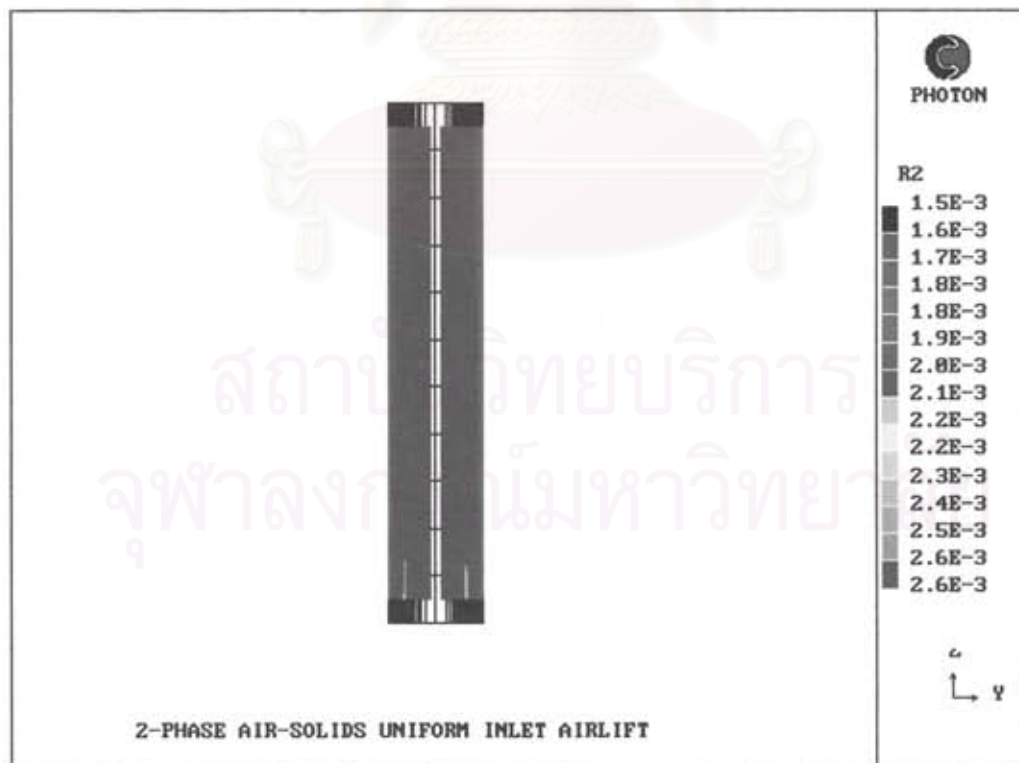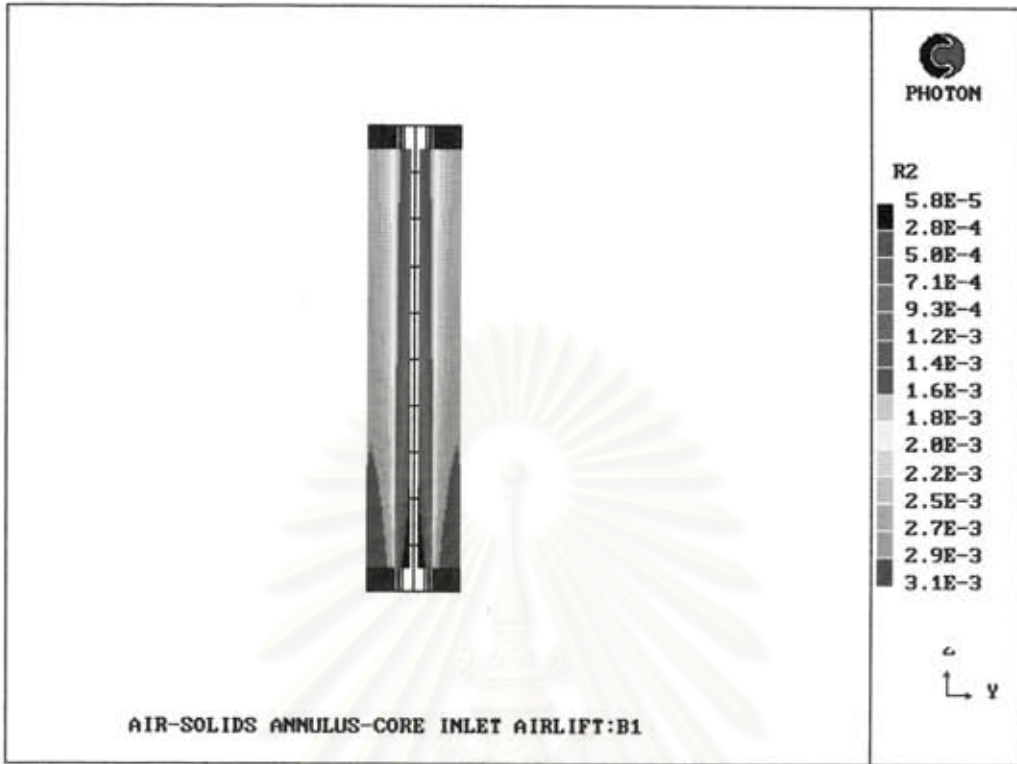from NZ=20 to NZ=30 (Zmin =1.90m ,Zmax=3.00 m)

Figure 6.13
Solid volume fraction contour line for case A (uniform inlet)
from NZ=30 to NZ=40 (Zmin =2.90m ,Zmax=4.00 m)

Figure 6.14
Solid volume fraction contour line for case B (mixture-annulus inlet)
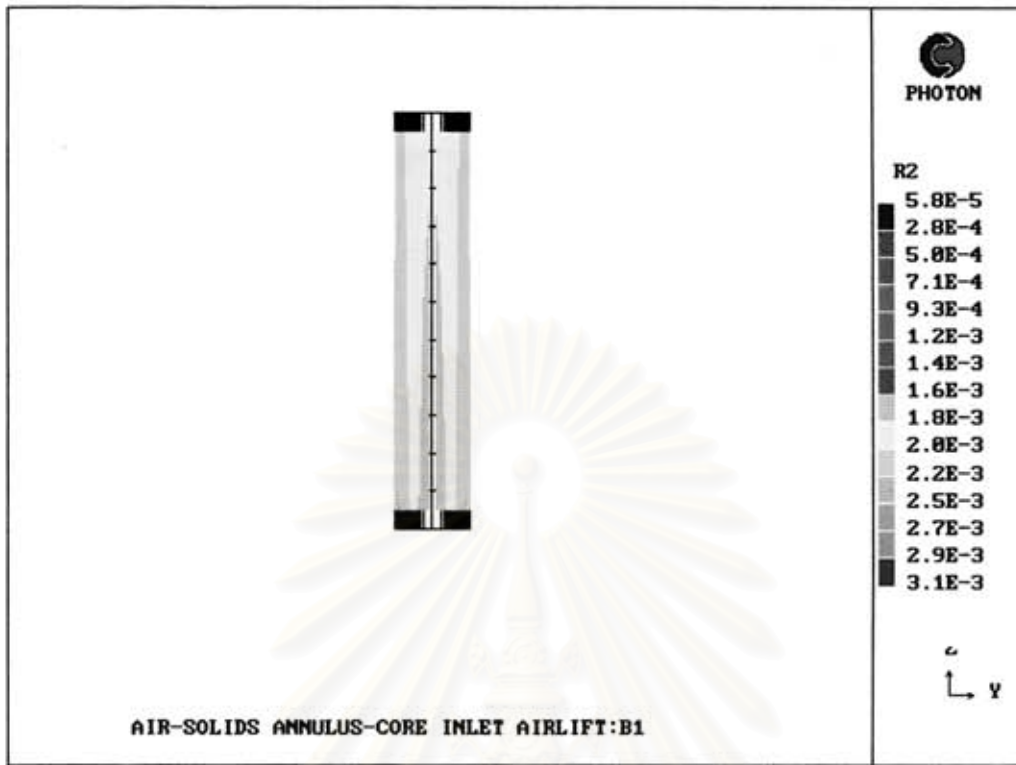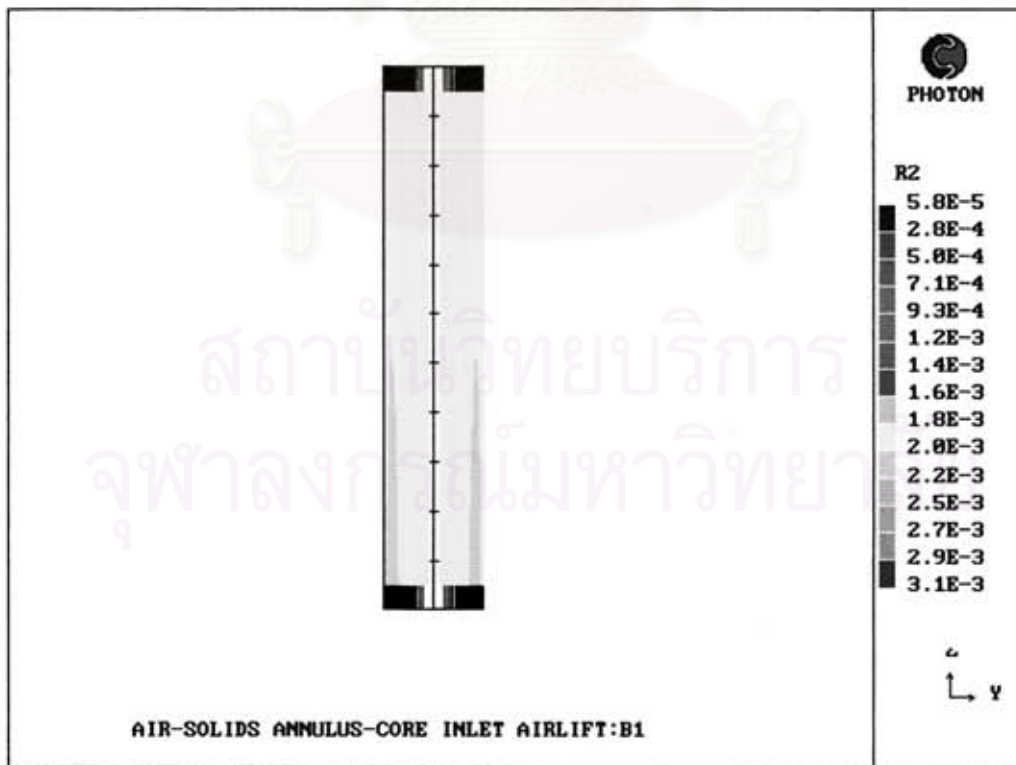From NZ=1 to NZ=10 (Zmin=0.0m., Zmax=1.0m.)
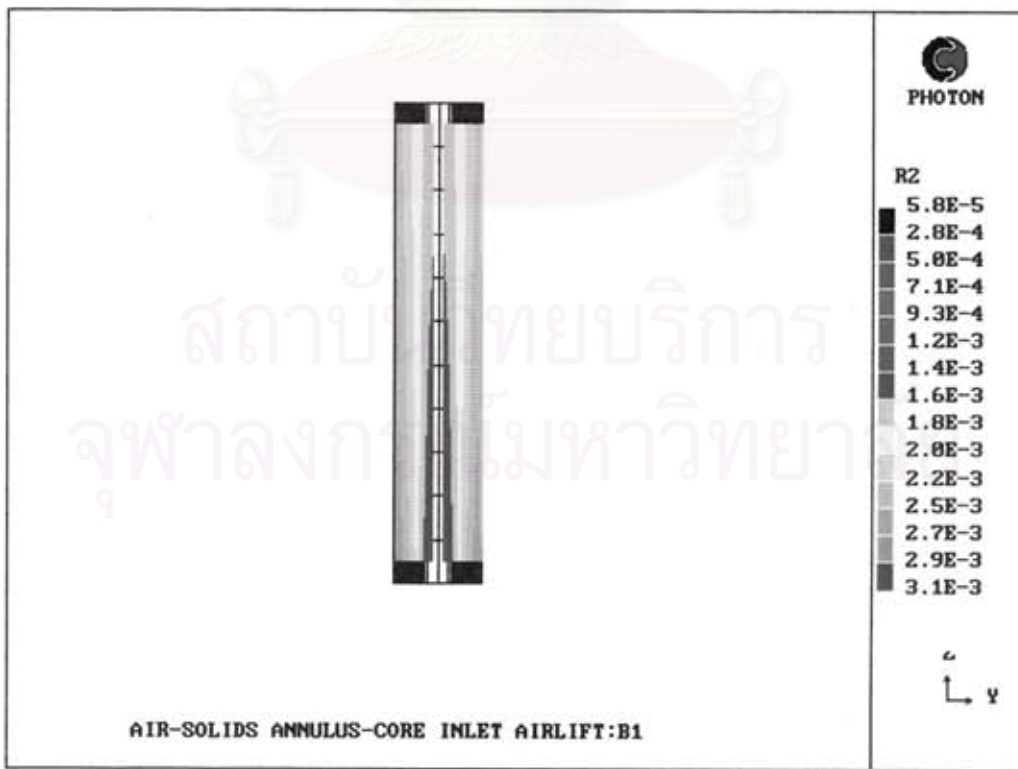
Figure 6.15
Solid volume fraction contour line for case B (mixture-annulus inlet)
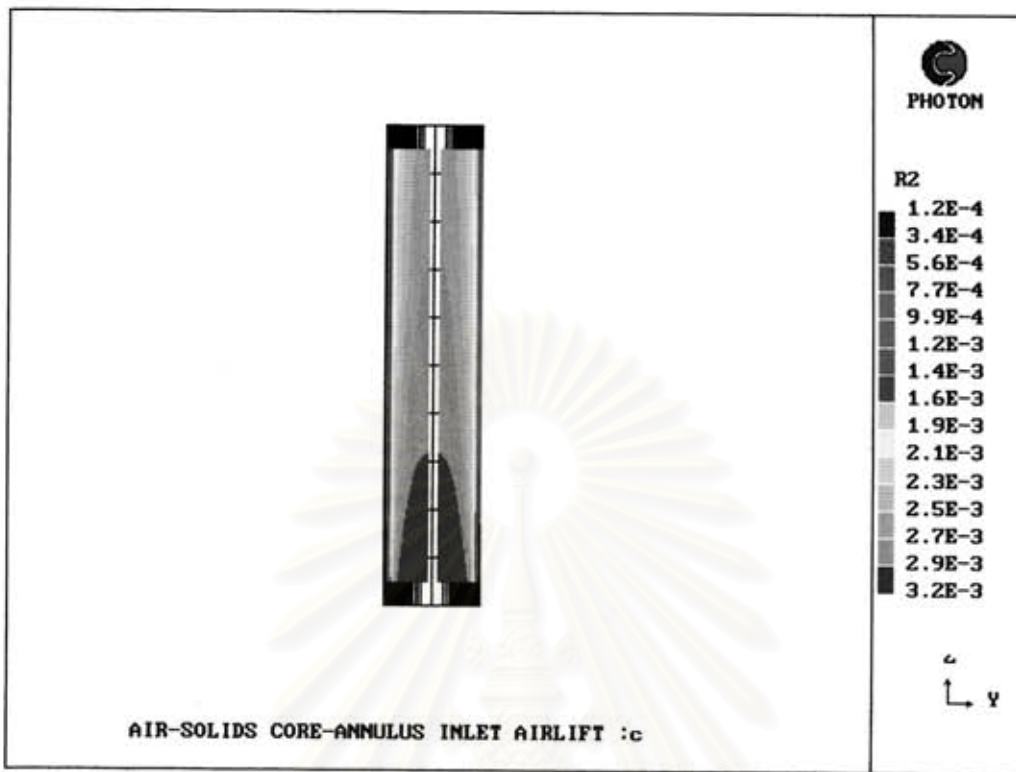From NZ=10 to NZ=20 (Zmin=0.9m., Zmax=2.0m.)

AIR-SOLIDS ANNULUS-CORE INLET AIRLIFT:B1

Figure 6.16
Solid volume fraction contour line for case B (mixture-annulus inlet)
From NZ=20 to NZ=30 (Zmin=1.9m., Zmax=3.0m.)

AIR-SOLIDS ANNULUS-CORE INLET AIRLIFT:B1

Figure 6.17
Solid volume fraction contour line for case B (mixture-annulus inlet)
From NZ=30 to NZ=40 (Zmin=2.9m., Zmax=4.0m.)

Figure 6.18
Solid volume fraction contour line for case C (mixture-core inlet)
From NZ=1 to NZ=10 (Zmin=0.0m., Zmax=1.0m.)
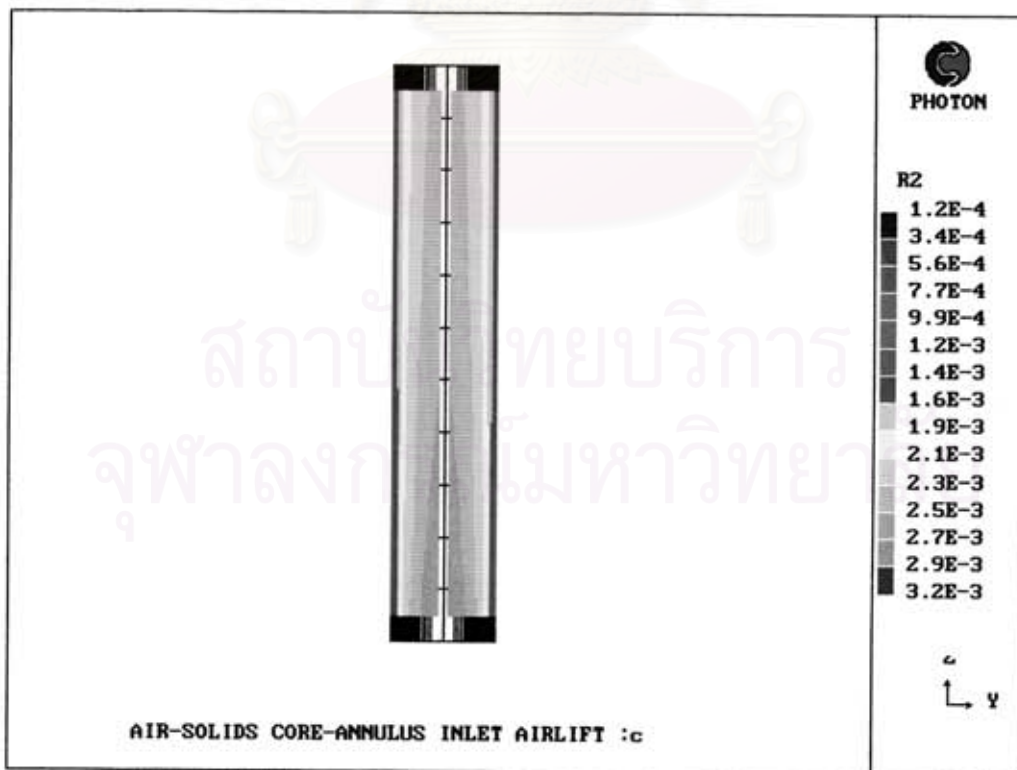

Figure 6.19
Solid volume fraction contour line for case C (mixture-core inlet)
From NZ=10 to NZ=20 (Zmin=0.9m., Zmax=2.0m.)

Figure 6.20
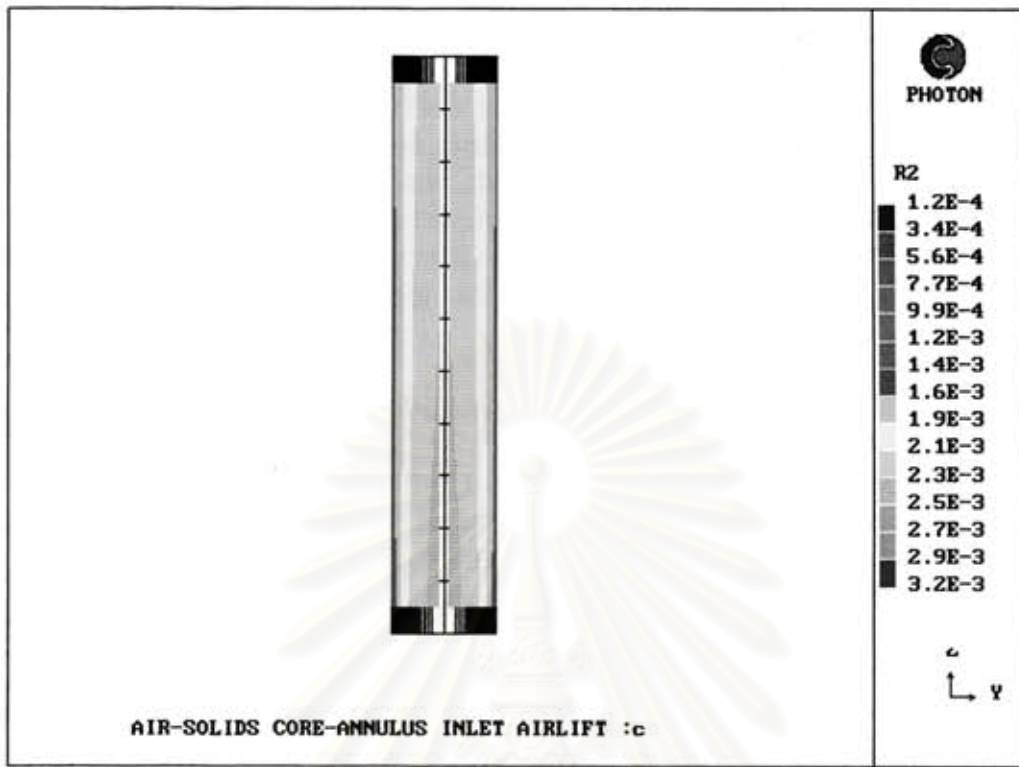Solid volume fraction contour line for case C (mixture-core inlet)
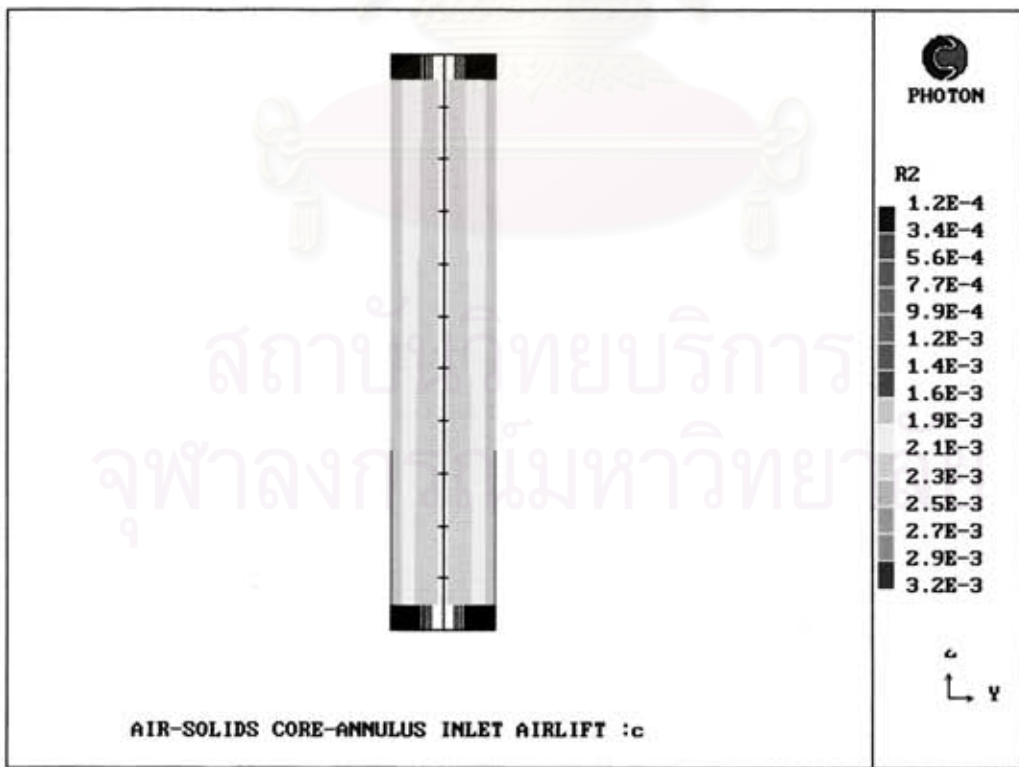From NZ=20 to NZ=30 (Zmin=1.9m., Zmax=3.0m.)

Figure 6.21
Solid volume fraction contour line for case C (mixture-core inlet)
From NZ=30 to NZ=40 (Zmin=2.9m., Zmax=4.0m.)

In Figure 6.22 the particle volume fraction of the computational cells attached to the wall of the three cases are plotted along axial direction. Mixture-core inlet (Case C) is the most favorable in the sense that it cause minimum particle volume fraction near wall in accelerating flow region relative to the other cases. Even though near-wall particle volume fraction profile which is minimum at the inlet gradually increase as the flow move upward due to mass diffusion, net resulting volume fraction profile is still superior to the profiles of other two cases. Uniform inlet (Case A) and mixture-annulus inlet (Case B) flow computations yield the same trend, the profiles of particle volume fraction attached to the wall are maximum at inlet and decrease along the axial direction.

6.5.2c. particle lift force at wall boundary

As discussed in Section 5.2a, particle Reynolds number (equation (3.36)) is a representative in analyzing the lift force (equation (6.3) and (6.4) ignoring air velocity gradient). The higher particle Reynolds number near wall, the higher possibility of lift, slipping and rebound of particles over the wall or deposited layer, as a result, lower possibility of sticking. As shown in Figure 6.23 particle Reynolds number profile of the computational cell attached to the wall of mixture-core inlet configuration case (Case C) is the highest among the three cases.

6.5.2d. Particle-wall collision rate

In Figure 6.24 collision rate index $\gamma_s \rho_s k^2/\varepsilon$ (equation(6.2)) of the three cases are plotted along axial direction. Again, mixture-core inlet configuration (Case C) simulation yields the most favorable results than the other two cases.
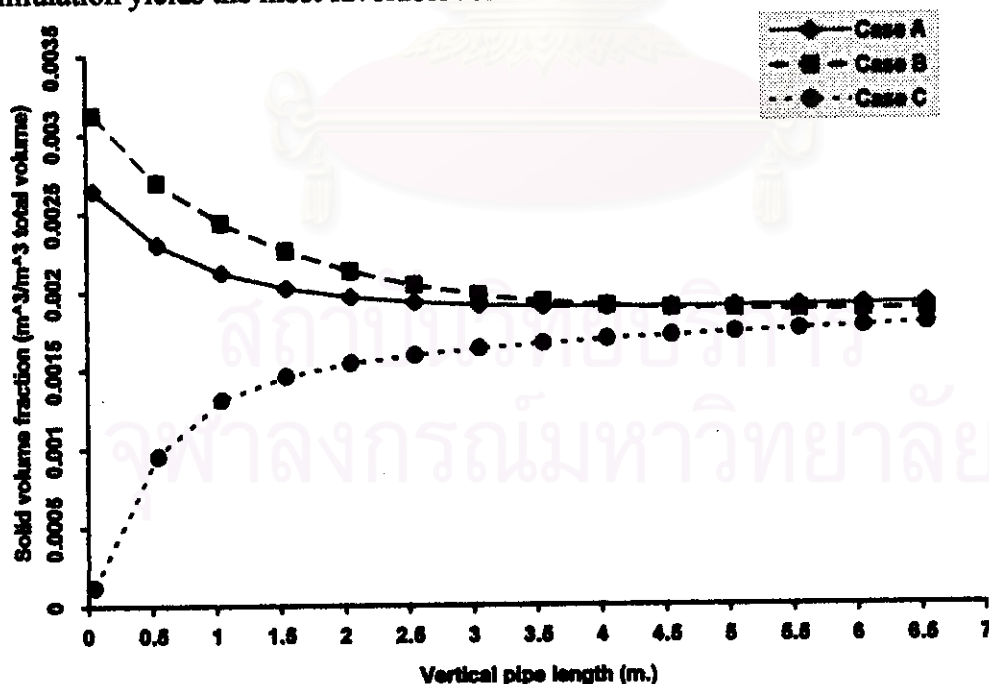
Figure 6.22
Particle volume fraction versus axial distance at the computational cell attached to the wall, cell width = 1.0 mm, cell node distance = 0.5 mm, from wall Data legend : Case A is uniform inlet ; Case B is mixture annulus inlet; case ;Case C is mixture-core inlet
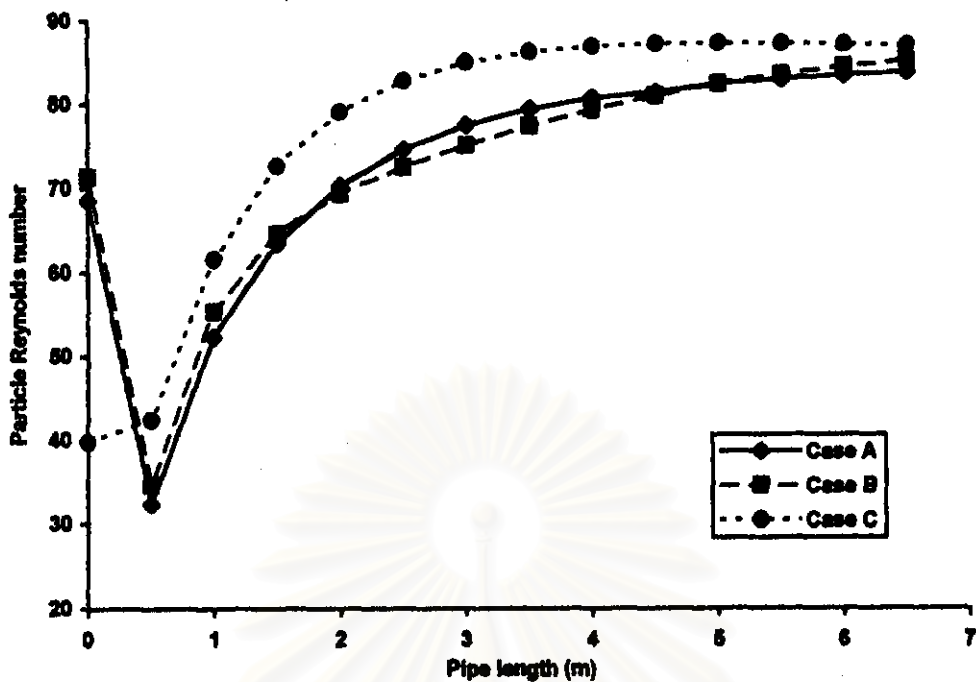
Figure 6.23
Particle Reynolds number versus axial distance at the computational cell attached to the wall
cell width = 1.0 mm, cell node distance = 0.5 mm, from wall Data legend : Case A is uniform
inlet ;Case B is mixture annulus inlet; case ;Case C is mixture-core inlet

Figure 6.24
$\gamma_{ao}k^2/\epsilon$ versus axial distance at the computational cell attached to the wall, cell width = 1.0
mm, cell node distance = 0.5 mm, from wall, Data legend : Case A is uniform inlet ;Case B is
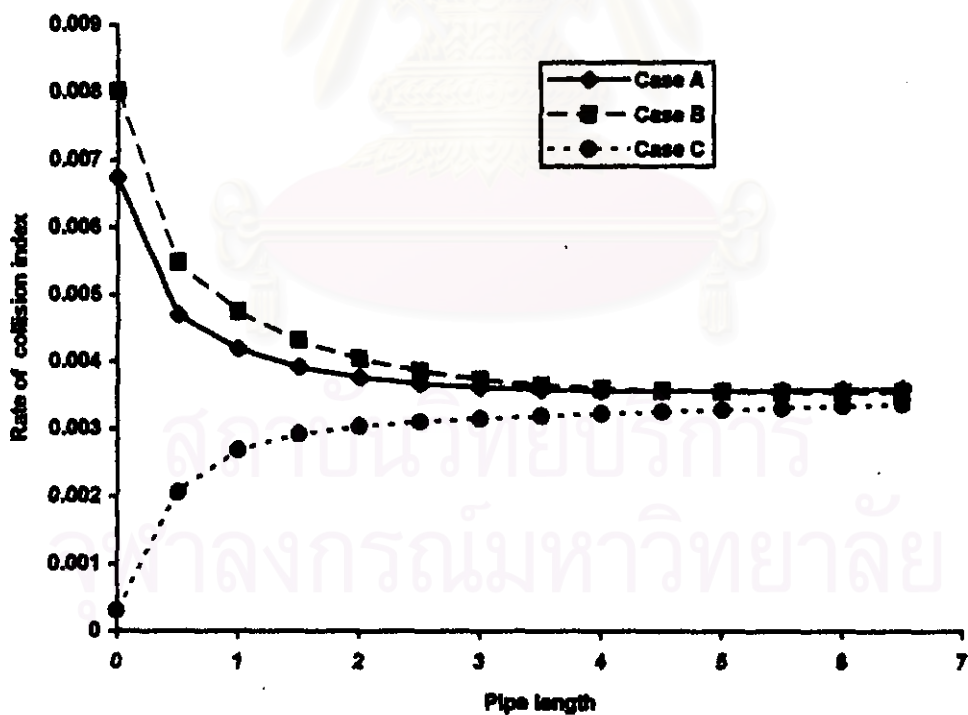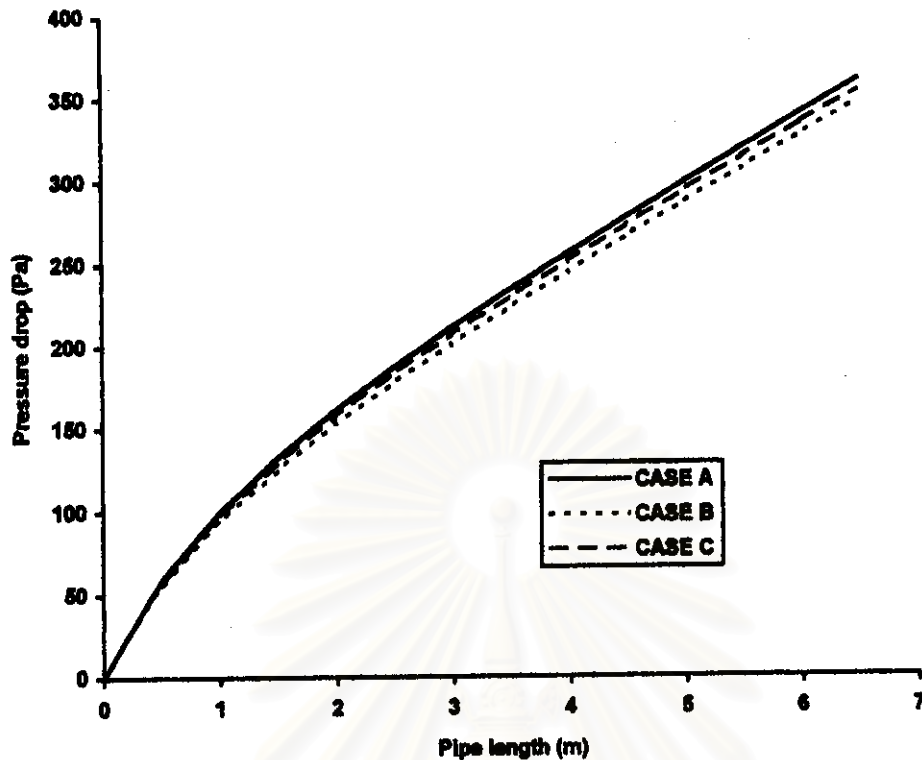mixture annulus inlet; case ;Case C is mixture-core inlet

Figure 6.25
Pressure drop profile versus axial distance . Data legend : Case A is uniform inlet :Case B is
mixture annulus inlet; case :Case C is mixture-core inlet

Comparing among the three cases, mixture-core inlet configuration (Case C)
perform the best task in minimizing deposition rate of powders on the airlift pipe
wall.

6.5.2e. Pressure drop profile

In Figure 6.25, pressure drop in axial direction of the three cases are plotted.
The profile of the three cases are almost similar since air velocity and total solid
loading ratio of all cases are equal . A conclusion can be established in observing the
pressure drop in Figure 6.25 that inlet configuration does not significantly affect to
pressure drop of the flow.

6.5.3 Effect of core area for mixture-core inlet configuration case.

According to particle-wall deposition evaluation of various inlet
configurations done in previous section, mixture-core inlet configuration simulation
yields superior flow field results in reduction of deposition rate on pipe wall. In this
section, effect of mixture-core inlet area variation to flow field will be investigated.

Computational details of varied mixture-core area case of mixture-core inlet
configuration (Case C+) are specified in Table 6.1 through 6.5. The mixture-core area
of Case C is 79.57% of total pipe area and , for Case C+, 64.3% of total area. The

local solid loading ratio is 1.507 for Case C and 1.8663 for Case C+ . The local solid loading ratio of Case C+ is reaching upper limit of model validation in Chapter 5.

Air and particle velocity profiles for Case C+ are not presented here since its trend are similar to Case C even though there are some quantitative difference. Particle volume fraction full-area contour plot of Case C+ are not also represented here by the same reason.

6.5.3a Particle volume fraction

In Figure 6.26 the particle volume fraction at the computational cell attached to the wall of the Case C and C+ is plotted against the reference case along axial direction. Lower particle volume fraction profile of Case C+ can be observed up to z=4.00 m . The particle volume fraction difference between Case C and C+ is insignificant after Z=5.00m .
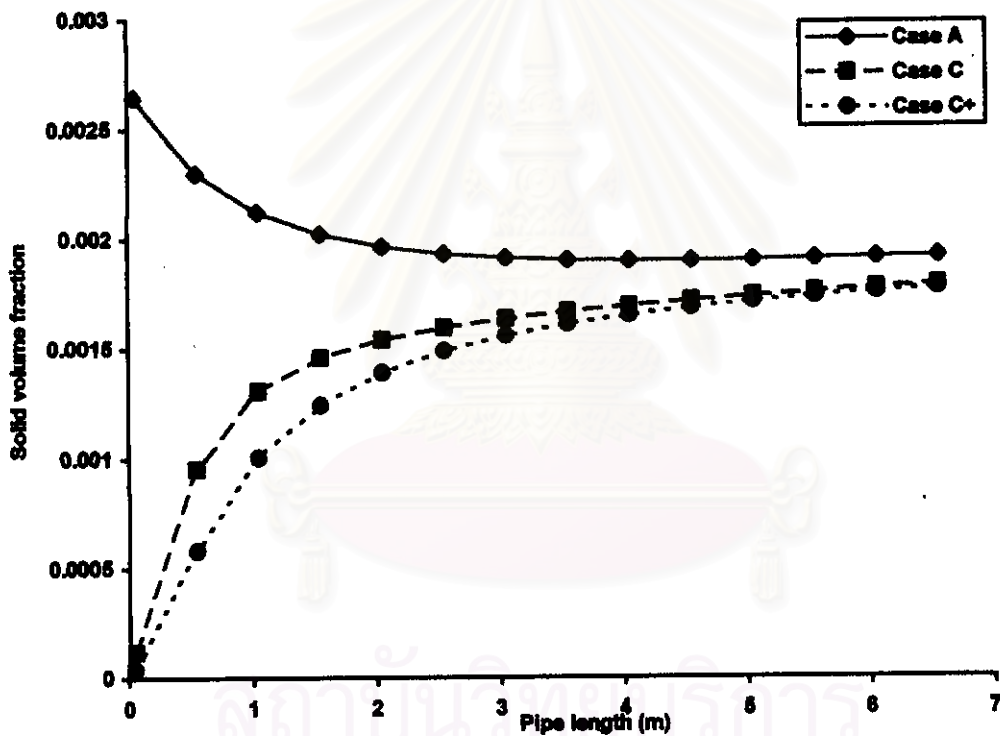

Figure 6.26

Particle volume fraction versus axial distance at the computational cell attached to the wall cell width = 1.0 mm, cell node distance = 0.5 mm, from wall Data legend : Case A is uniform inlet : Case C is mixture core inlet configuration as the condition detailed in table 6.5: case C+ is mixture-core inlet with varied mixture core area as the condition detailed in table 6.5. All cases are simulated at equal total solid loading ratio=1.2

6.5.3b. Particle lift force

In Figure 6.27 particle Reynolds number of Case C Case C+ and reference case at the computational cell attached to the wall are plotted along axial distance. Again, Case C+ show more favorable results against Case C in the aspect of lift force effect at the wall. The value seem to converge to same asymptotic value. Since the volume fraction of particle attached to the wall at the inlet of Case C+ is smaller than of Case C at equal air velocity, the resulting particle velocity is therefore larger. The higher particle velocity is major factor which induce particle Reynolds number of Case C+ to be larger than Case C. As a result, lift force of Case C+ is higher than Case C.

6.5.3c. Particle-wall collision rate

In Figure 6.28 collision rate index $\gamma_p \rho_p k^2/\varepsilon$ (equation(6.2)) of Case C, C+ and reference case are plotted along axial direction . The trend of curves in Figure 6.28 are analogous to particle volume fraction curves in Figure 6.25. The particle collision rate index of Case C+ is significantly lower than of the Case C up to z=4.0 m. The collision index curve of Case C is steeper than of Case C+ from z=0 to z=2.50m which indicate the higher strength of phase mass diffusion of particle from core area toward the pipe wall in this region. After z=2.5 m, the slope of collision rate curve of Case C is nearly constant while slope of collision rate of Case C gradually decrease until reaching constant at Z=5.00 m.
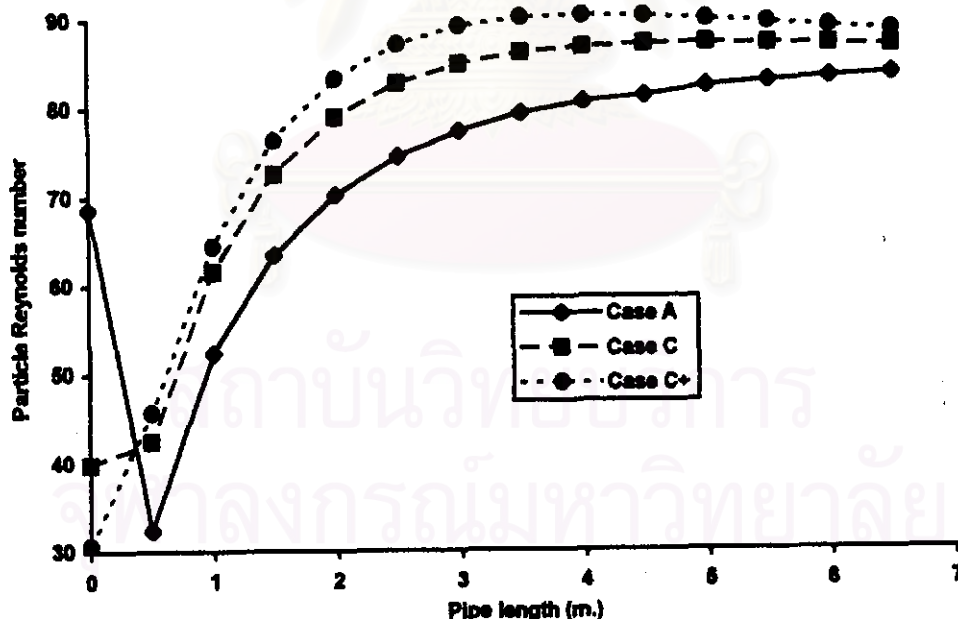

Figure 6.27

Particle Reynolds number versus axial distance at the computational cell attached to the wall cell width = 1.0 mm, cell node distance = 0.5 mm. from wall Data legend :Case A is uniform inlet configuration: Case C is mixture core inlet configuration as the condition detailed in table 6.5: case C+ is mixture-core inlet with varied mixture core area as the condition detailed in table 6.5. All cases are simulated at equal total solid loading ratio=1.2
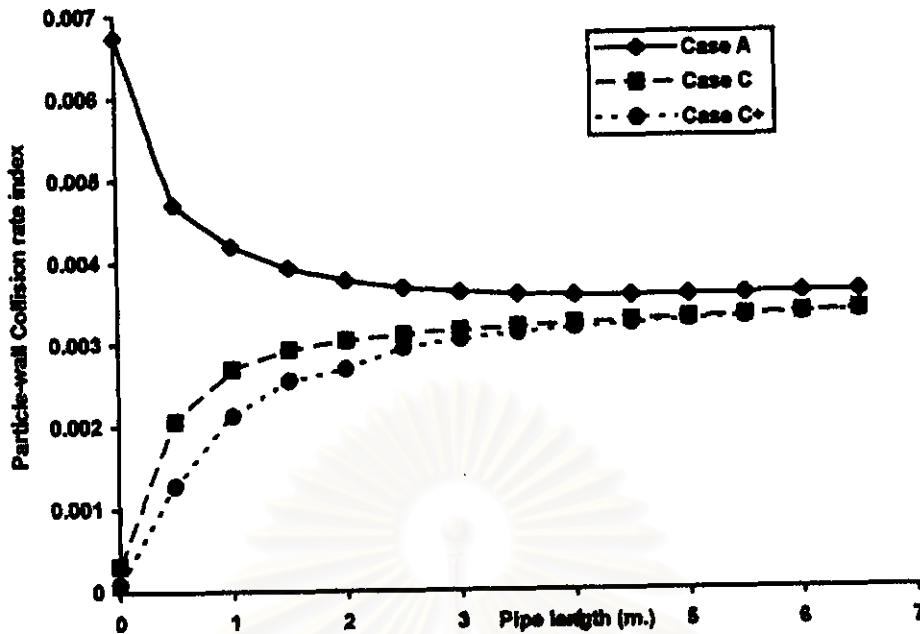
Figure 6.28

$\gamma_p \Theta_p k^2 / \varepsilon$ versus axial distance at the computational cell attached to the wall, cell width = 1.0 mm, cell node distance = 0.5 mm, from wall. Data legend : Case A is uniform inlet configuration; Case C is mixture core inlet configuration as the condition detailed in table 6.5; case C+ is mixture-core inlet with varied mixture core area as the condition detailed in table 6.5. All cases are simulated at equal total solid loading ratio=1.2

Figure 6.29

Pressure drop profile versus axial distance . Data legend : Case C is mixture core inlet configuration as the condition detailed in table 6.5; case C+ is mixture-core inlet with varied mixture core area as the condition detailed in table 6.5. All cases are simulated at equal total solid loading ratio=1.2
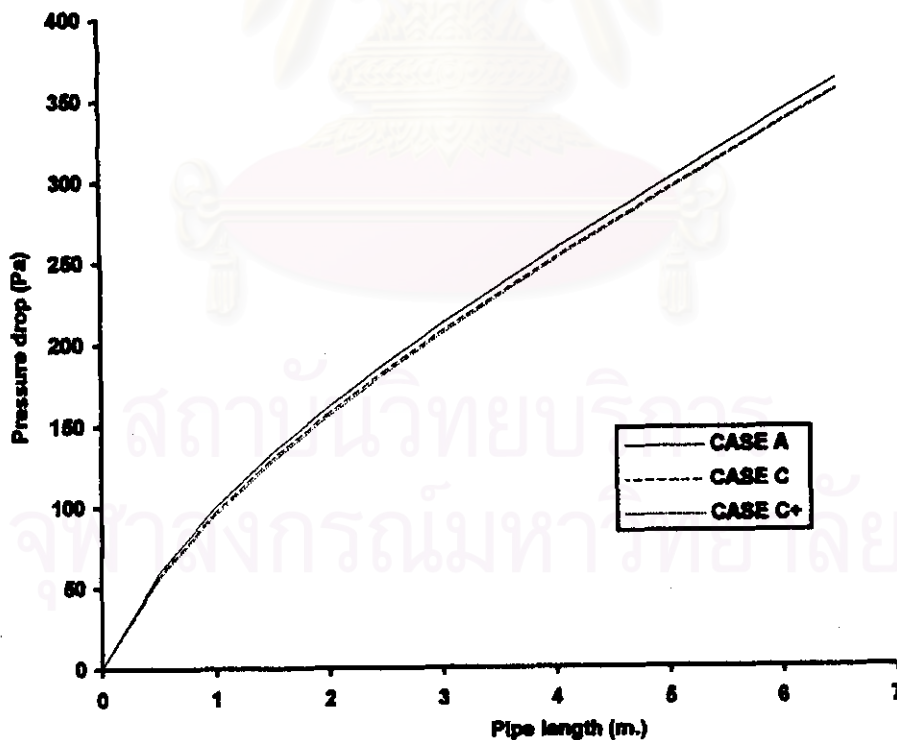
In Figure 6.29, pressure drop of Case C and C+ together with reference case are plotted along axial direction.It can be clearly seen that change of mixture-core inlet area does not affect to the axial pressure drop profile.

The flow field result of Case C+ is superior to Case C in view of particle-wall deposition reduction in the starting section ($0 < z < 4.00m$) but nearly equal after $z > 4.00m$. The results of simulation lead to the conclusion that rate of particle deposition decrease as the mixture-core inlet area decrease. The lower limit of mixture-core area can not be determined by this simulation as the limit depend on particle pick up capability and particle inlet velocity which is expected to be lower at the higher solid loading ratio. Plant scale experiment is still required to optimize the mixture-core area. In preliminary plant scale test, Case C inlet configurations is suggested due to its safer flow parameter and satisfactory predicted performance.